

## Chapter 1

# The Cassini-Huygens Mission

### 1.1 Overview

The *Cassini-Huygens* mission (hereafter known as *Cassini*) was a space mission designed to investigate the Saturn system, and was a collaboration between NASA, ESA and the Italian Space Agency (ASI). It was composed of a main *Cassini* orbiter spacecraft with 12 instruments on board, and the *Huygens* probe with a further 6, as described in ?. A diagram of this spacecraft is shown in Figure 1.1. The instruments particularly relevant to the work in this thesis are discussed later in this chapter.

Together, these instruments were designed such that the mission could investigate the entire Saturn system, from the planet itself to its atmosphere, rings, moons, and magnetosphere. The moon Titan was one of the key focuses of the investigation, as it is the only moon in the solar system with a significant atmosphere, and it was initially thought to be a key source of plasma for the magnetosphere. The *Huygens* probe was therefore designed to detach from the main *Cassini* orbiter and make a single trajectory by parachute down to the surface of Titan, making *in situ* measurements of Titan's atmosphere during the descent. The shield covering the *Huygens* probe before it was deployed can be seen in Figure 1.1.

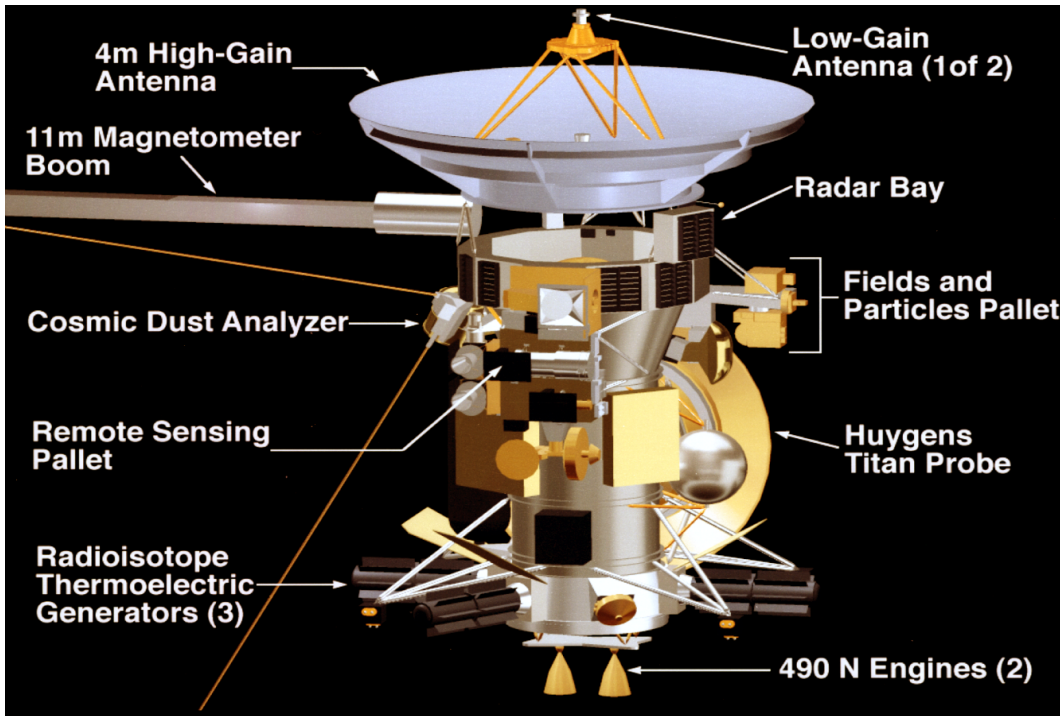


**Figure 1.1:** Diagram of the *Cassini-Huygens* spacecraft, from ?. The spacecraft is about 6.8 m in height.

## 1.2 Mission Timeline

*Cassini* launched from Cape Canaveral in Florida in October 1997, and finally arrived at the Saturn system in July 2004, after gravity-assist flybys of Venus, Earth and Jupiter. The mission was initially designed to operate for four years, from 2004-2008, and during this ‘Prime Mission’ *Cassini* completed 75 orbits of Saturn, and 44 flybys of Titan. The Prime Mission was incredibly successful, resulting in many exciting and unexpected discoveries about the Saturn system, such as the plumes of water being ejected from the icy moon Enceladus (?).

The mission was then extended by two years; the ‘Equinox Mission’. This extension allowed *Cassini* to observe how the behaviour of the Saturn system changed with season, from northern winter to northern spring. Saturn’s obliquity relative to the ecliptic plane is  $26.7^\circ$ . As discussed in Section ??, a Saturn year lasts 29 years, and the northern spring equinox occurred in August 2009, near the middle of the Equinox Mission. From a magnetospheric

science perspective, equinox is a particularly interesting time to investigate the Saturn system, as the incident solar wind direction is parallel to Saturn’s rotational/dipole equator, rather than at an angle slightly above or below. This means the solar wind conditions are approximately symmetrical in the northern and southern hemispheres, allowing for certain hemispheric effects, such as those discussed in Section ??, to be more readily investigated. Indeed, the data that is analysed in this thesis, particularly in Chapter ??, were measured during *Cassini’s* Equinox Mission.

The mission was then further extended from 2010-2017, known as the ‘Solstice Mission’, as the Saturn year continued into northern summer solstice in May 2017. The spacecraft trajectories were optimised to provide the most extensive coverage of scientifically interesting areas of the Saturn system, in the context of the entire mission. This culminated in the Grand Finale’s ‘Proximal Orbits’, from April to September 2017. In each of these 22 final orbits, *Cassini* traversed the gap between Saturn’s atmosphere and the innermost ring, therefore orbiting far closer to the planet than at any other time in the mission. This provided the opportunity to investigate scientific mysteries that still had not been answered from mission data so far, such as the core rotation rate of the planet and internal magnetic field structure. The *Cassini* mission then ended on 15 September 2017, as the spacecraft plunged into the planet’s atmosphere and lost contact with Earth. The Grand Finale was designed in this way not just for maximum scientific reward, but also because the onboard rocket propellant used to manoeuvre the spacecraft was running out. With *Cassini’s* discovery of a likely sub-surface water ocean at Enceladus, and also prebiotic chemistry at Titan, the mission could not risk the spacecraft accidentally crashing into one of these moons and potentially contaminating them with Earth-based life forms. It was therefore necessary to deliberately crash the spacecraft into the planet Saturn itself.

Figure 1.2 shows an overview of the entire *Cassini* mission. At the top of the image the trajectories of the orbits are depicted, showing the extensive

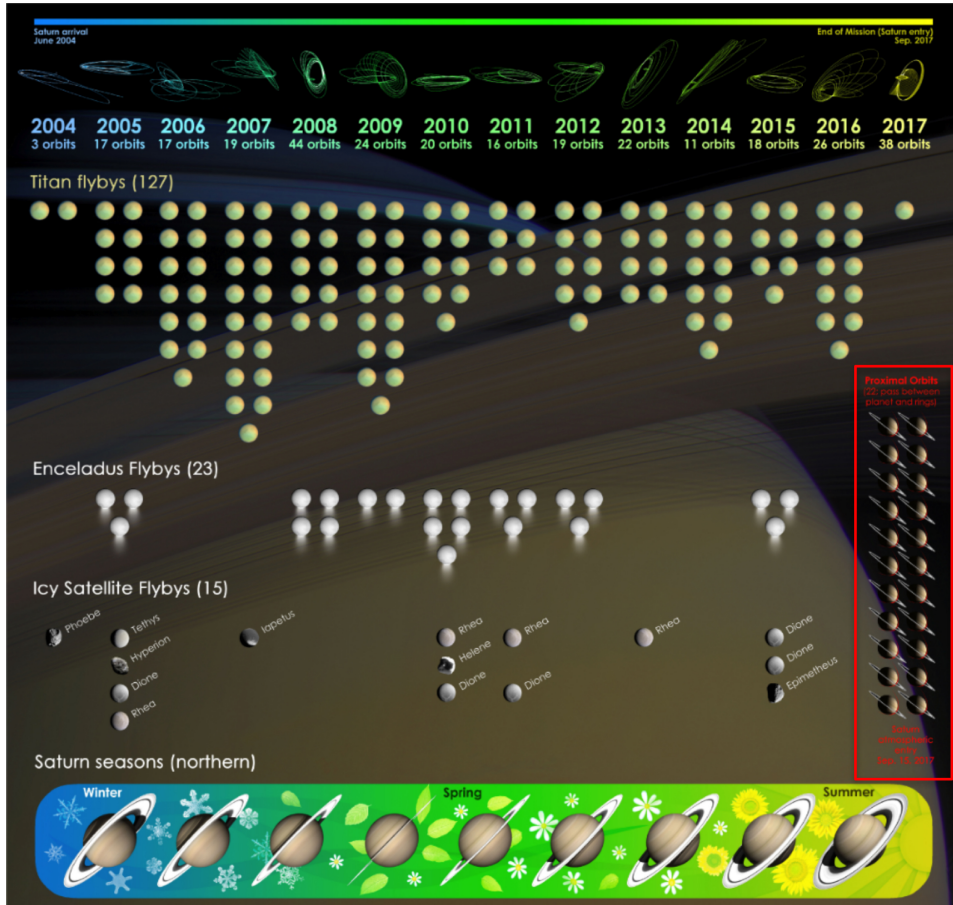


**Figure 1.2:** Diagram showing overview of *Cassini* space mission orbit trajectories and moon flybys, from ?.

coverage *Cassini* made in radial distance, latitude and local time. Also shown are the number of flybys of various moons, and at the bottom the Saturn season is depicted. The proximal orbits, shown in red, are barely visible as they are so close to the Saturn surface.

## 1.3 Key Instruments

### 1.3.1 Magnetometer (MAG)

The dual technique magnetometer system (MAG) measured the magnitude and direction of Saturn's magnetic field *in situ*, described in ? and summarised here. The system was composed of a Vector/Scalar Helium Magnetometer (V/SHM), located at the end of the 11 m long boom shown in Figure 1.1, and a Fluxgate Magnetometer (FGM), located half way along it. This position-

ing was chosen so that measurements were contaminated as little as possible by magnetic fields generated by other instruments and electronics subsystems onboard the spacecraft itself, and also so that measurements from the two instruments could be compared for calibration. However the V/SHM malfunctioned early on in the mission, in November 2005, and so all the data presented in this thesis were measured solely by the FGM.

The FGM was composed of three fluxgate sensors positioned orthogonal to each other, to measure the three vector components of the ambient magnetic field. In each sensor, a coil of wire ('drive winding' in Figure 1.3) was wound around a ring-shaped core made of highly magnetically permeable alloy. A 15.625 Hz square wave current flowed through this drive coil, in order to induce a magnetic field in the core until it was saturated, with clockwise orientation as shown by the pale arrows. Surrounding this entire set up was another coil of wire ('measurement winding' in Figure 1.3). In the absence of an external magnetic field, the two halves of the core shown in Figure 1.3 would go into and out of saturation at the same time due to the drive winding current, and so there would be no change of flux through the measurement winding. However in the presence of an external magnetic field oriented as shown by the green arrow, one half of the core would become saturated more quickly than the other depending on the phase of the drive winding current, causing a net change in magnetic flux through the measurement winding. In accordance with Faraday's law of induction, this would induce a voltage in the measurement winding, which could then be calibrated and used to measure the magnitude of the external magnetic field. Only the component of the magnetic field perpendicular to the measurement winding orientation can be detected by this process, hence the need for three orthogonally positioned sensors. These three sensors were mounted on a single ceramic block, with the entire FGM instrument weighing just 0.44 kg. The material ceramic was chosen for its low thermal expansion coefficient, meaning it changes shape very little under changes in ambient temperature, and so any misalignment between the sensors

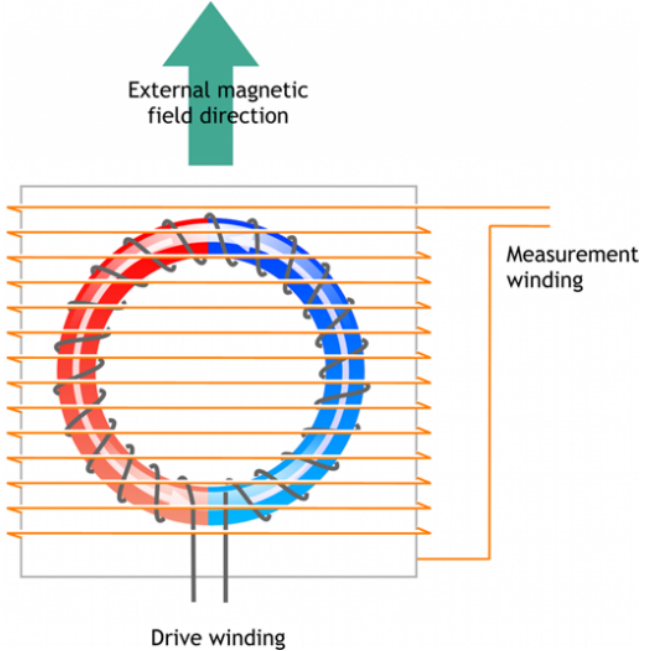


**Figure 1.3:** Diagram showing basic construction of a fluxgate magnetometer, from ?. The drive winding and measurement winding are shown in dark grey and orange, respectively. The magnetic field induced in core due to the current in the drive winding is shown by the pale arrows on top of the blue and red halves of the core. The external magnetic field direction is shown by the large green arrow.

was minimised.

The FGM had multiple operational ranges depending on the likely ambient magnetic field strength, which it could switch between automatically, and had a digital resolution of approximately one part in 10,000 depending on the range. The four ranges were  $\pm 40 \text{ nT}$ ,  $\pm 400 \text{ nT}$ ,  $\pm 10\,000 \text{ nT}$ , and  $\pm 44\,000 \text{ nT}$ , necessarily for sampling different regions of the magnetosphere and space environment, where the magnetic field strength varies over many orders of magnitude. The normal downlink data rate for the FGM was 32 vectors/s, although in this thesis we only investigate large-scale magnetospheric structures on large timescales, and so only present 1-hour-averaged MAG data. *In situ* observations of Saturn's magnetic field can reveal detailed information about the structure of Saturn's magnetosphere, such as the dynamical current sheet behaviour (e.g. ?), and was also used to demonstrate the existence of an atmospheric plume at the icy moon Enceladus (?).

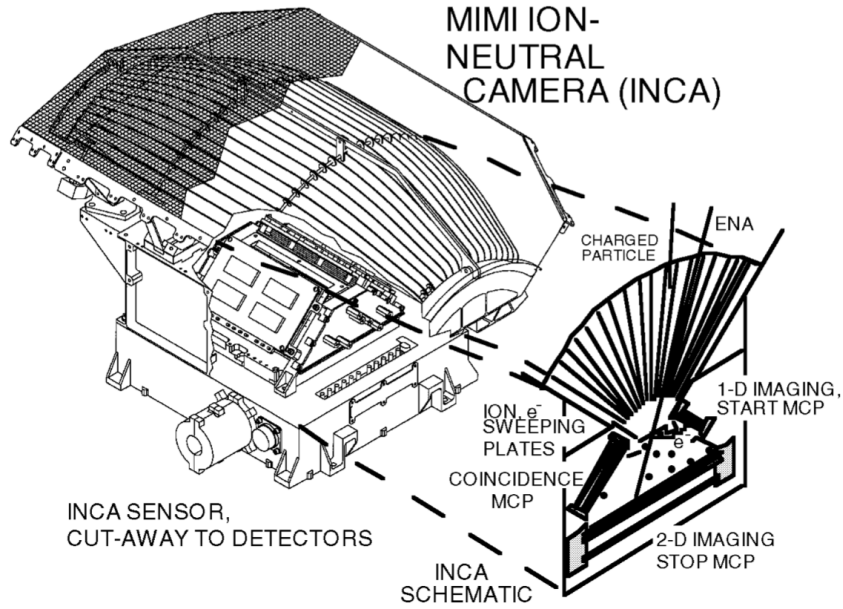


**Figure 1.4:** Cutaway diagram of the MIMI/INCA instrument, from ?.

### 1.3.2 Magnetospheric Imaging Instrument (MIMI)

The Magnetospheric Imaging Instrument (MIMI) was a system for detecting both neutral and charged particles with high energies, described in ? and summarised here. It was composed of three separate instruments, each described below.

#### 1.3.2.1 Ion and Neutral Camera (INCA)

The Ion and Neutral Camera (INCA) was designed to detect both energetic neutral atoms (ENAs) and ion species over the range of energies  $0.007 - 3 \text{ MeV/nucleon}$ , and use time-of-flight information to determine the particle's energy and incident direction. A simple diagram of the instrument is shown in Figure 1.4.

Particles detected by the instrument would arrive broadly from above in the frame of in Figure 1.4, and pass through the fan-like arrangement of serrated collimator plates, labelled as ‘ION,  $e^-$  SWEEPING PLATES’. When in ‘neutral mode’, these plates would be alternately charged at  $\pm 6 \text{ kV}$  in order to sweep any energetic charged particles (with energies  $\leq 500 \text{ keV}$ ) into the plate walls, thus excluding them from the internal detector. ENAs meanwhile

would pass through the region unperturbed, and then penetrate a thin foil layer covering the entrance slit. This would generate secondary electrons in the foil, which are steered to a 1-D microchannel plate (MCP) labelled as ‘1-D IMAGING, START MCP’ in Figure 1.4, recording the entrance position of the ENA and start time of travel. As the ENA proceeded further to the back of the instrument, it would penetrate another thin foil layer and encounter a 2-D microchannel plate, labelled ‘2-D IMAGING STOP MCP’, recording the exit position (in 2-D) and the end time of travel. At the same time, secondary electrons generated in the second thin foil layer would be steered to the labelled ‘COINCIDENCE MCP’ microchannel plate, in order to reduce background measurement noise by comparing the detection with those of the other plate. From all this information, the energy, mass, and incident direction of the ENA could be deduced. In particular it was found that the number of electrons generated in the foil was proportional to the mass of the incident particle, which enabled the species (e.g. oxygen or hydrogen) of the particle to be determined. When operating in ‘ion mode’, the charge on the sweeping plates would be switched to zero and the instrument would detect ion species in a similar way.

At Saturn, ENAs can be produced via charge exchange between singly-charged energetic ions and Saturn’s neutral gas distribution (which originates from Saturn’s rings and moons). Through collisions, an energetic ion can ‘steal’ an electron from a neutral particle, such that the ion becomes neutral and is no longer constrained by the planetary magnetic field, and so then travels through space unperturbed. The energetic ions that make up Saturn’s equatorial ring current can therefore be traced remotely via detection of ENAs originating from the equatorial plane. Figure 1.5 shows such an ENA image taken by *Cassini’s* MIMI/INCA instrument on 19 March 2007, clearly showing the variable and substantial ring current structure.

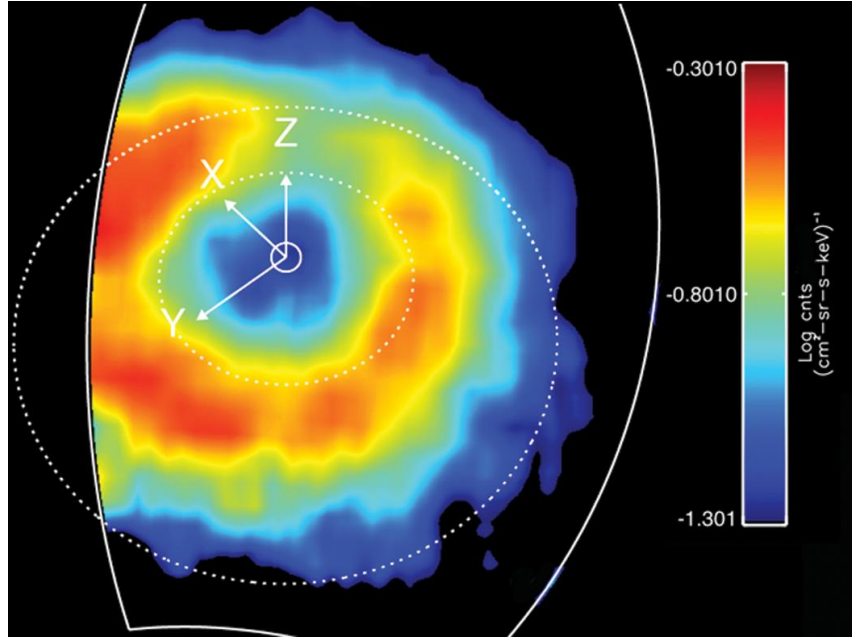


**Figure 1.5:** ENA image of Saturn's ring current from the MIMI/INCA instrument as viewed from a latitude of 55° above the northern hemisphere, averaged over a 3 hour period on 19 March 2007. Colour shows ENA intensity as per the colour bar. Saturn is at the centre, and the white dashed lines show the orbits of the moons Rhea ( $8.7 R_S$ ) and Titan ( $20.2 R_S$ ). The Z axis points along Saturn's dipole/spin axis, the Y axis points approximately towards dusk, and the X axis points approximately towards the Sun. The MIMI/INCA field of view is shown by the solid white line.

### 1.3.2.2 Charge-Energy-Mass Spectrometer (CHEMS)

The CHEMS instrument was designed to measure the charge, energy and mass of energetic ions, in the energy range 3 – 220 keV/e, using electrostatic deflection and time-of-flight information. The mounting of the instrument on the fields and particles pallet labelled in Figure 1.1, and the construction described below, meant that during a spacecraft roll it would have almost  $4\pi$  steradians viewing geometry. This enabled the capability of measuring 3-D distribution functions of the energetic ion populations. A diagram of the instrument is shown in Figure 1.6.

As an ion entered the instrument, it would first encounter the 'Deflection System', consisting of two oppositely charged spherical plates as shown in the diagram. The voltage across the plates was stepped through a series of logarithmically spaced values over time to a maximum of  $\pm 9.2$  keV, such

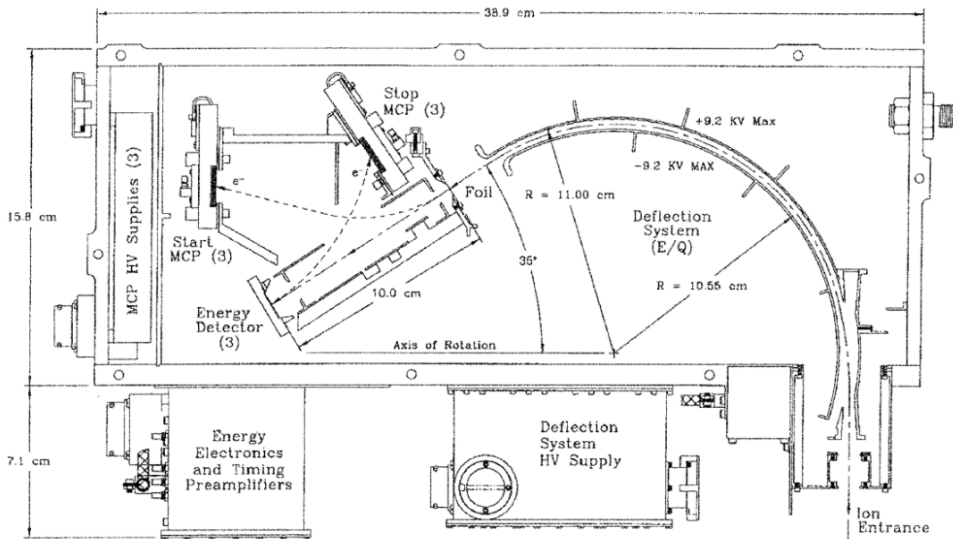


**Figure 1.6:** Diagram of the MIMI/CHEMS instrument, from ?.

that the plates acted as an energy per charge ( $E/Q$ ) filter, allowing only ions within a small ( $\sim 3\%$ )  $E/Q$  band to pass through the system at any given time. If transmitted, the ion would then penetrate a thin foil layer, generating secondary electrons that are steered to the labelled ‘Start MCP’, which would enable a time-of-flight calculation to be made as in MIMI/INCA. The ion would then impact the solid-state detector, labelled as ‘Energy Detector’ in Figure 1.6, generating secondary electrons that are steered to the ‘Stop MCP’, for the time-of-flight calculation. The solid-state detector also measured the residual energy of the ion, so that the charge be ascertained from the initial  $E/Q$  measurement. Three independent telescopes with different viewing angles were included in CHEMS, hence the ‘(3)’ labels, in order to enable the aforementioned coverage of viewing geometry.

In combination with the other instruments that make up MIMI, MIMI/CHEMS was used to detect the widespread presence of energetic oxygen ( $O^+$ ) and hydrogen ( $H^+$ ) ions in Saturn’s equatorial magnetosphere, and determine the partial pressures associated with the two populations independently. (e.g. ?). The influence of his hot plasma population on the large-scale structure of the magnetosphere is discussed and investigated at length in this thesis, in particular in Chapters ?? and ??.

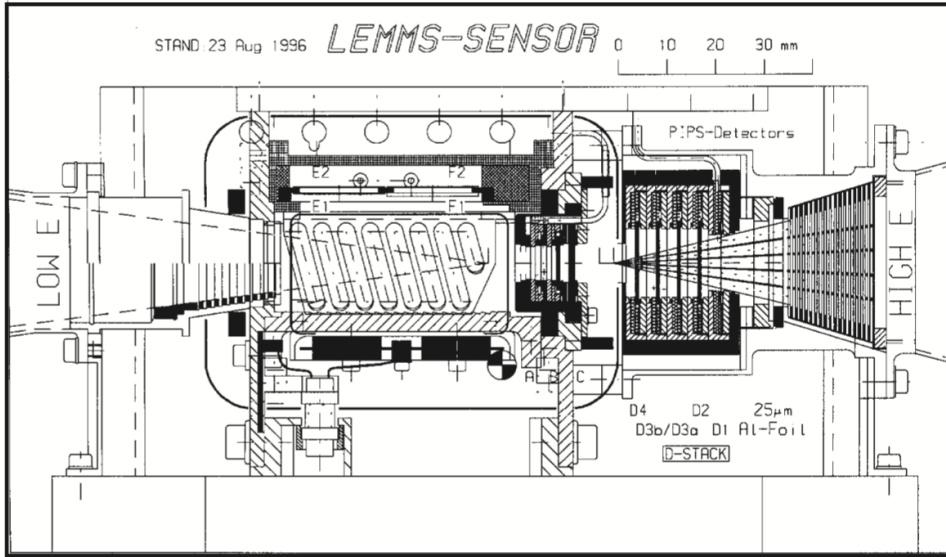


**Figure 1.7:** Diagram of the MIMI/LEMMS instrument, from ?.

### 1.3.2.3 Low-Energy Magnetospheric Measurement System (LEMMS)

The LEMMS instrument was designed to measure the distribution of energetic ion and electron fluxes. The instrument consisted of two oppositely oriented telescopes; a low-energy end, which measured ions with  $E > 30 \text{ keV}$  and electrons with  $E = 15 \text{ keV} - 1 \text{ MeV}$ , and a high-energy end, which measured ions with  $E = 1.5 - 160 \text{ MeV}$  and electrons with  $E = 0.1 - 5 \text{ MeV}$ . The entire assembly was shielded with a platinum cover to avoid particles with energies  $E < 30 \text{ MeV}$  penetrating the sides of the instrument. The instrument was mounted on a rotating platform to enable a larger total field of view; however, this became stuck early on in the mission in early 2005, and so it remained in a fixed orientation with field of view closely aligned with one of the MIMI/CHEMS telescopes for the remainder of the mission. A diagram of the instrument is shown in Figure 1.7.

In the low-energy telescope, an internal permanent magnet provided an inhomogeneous magnetic field, which separated the incoming ions and electrons that had passed into the instrument through the initial collimator. The electrons would be more strongly perturbed by the magnetic field, and so would

be diverted to the semiconductor silicon detectors labelled E(1,2) and F(1,2), depending on their initial energies and incident directions. Meanwhile ions, which are less strongly perturbed due to their higher mass (as discussed in this thesis, Section ??), proceeded to the back of the instrument and would strike the detectors labelled A and B. Data from the detectors could then be used to determine the energies of the incoming particles. In the high-energy telescope, a stack of detectors labelled D(1,2,3a,3b,4) detected incoming ions and electrons that had passed through the initial collimator on that side (plus a thin layer of aluminium foil, labelled ‘Al-Foil’, included to prevent contamination from sunlight and lower energy ions). The combination of detections from the different detectors, which had different electronic thresholds, could then be used to distinguish ions and electrons. Between detectors B and D4, a gold absorber labelled C was included to prevent lower energy ions penetrating through to the high-energy detectors.

Information from this instrument was used in combination with MIMI/INCA and MIMI/CHEMS to make measurements of the high energy plasma population in Saturn’s magnetosphere.

### 1.3.3 Plasma Spectrometer (CAPS)

The CAPS instrument was measure the of distributions ions and electrons at lower energies than those observed by the MIMI instrument, and is described in ? and summarised here. It was made up of three separate sensors, including an electron spectrometer (ELS), ion mass spectrometer (IMS), and ion beam spectrometer (IBS), which is not discussed here as was not used to make observations relevant to this thesis. ELS could detect electrons with energies in the range 0.6–29 000 eV, and IMS could detect ions in the range 1–50 000 eV. A diagram of the instrument is shown in Figure 1.8. The entire instrument was mounted on a rotating platform on the underside of the ‘fields and particles pallet’ shown in Figure 1.1, such that it had almost  $2\pi$  steradians field of view, when not partially blocked by other parts of the spacecraft.

At both ELS and IMS, incoming particles first travelled between separated

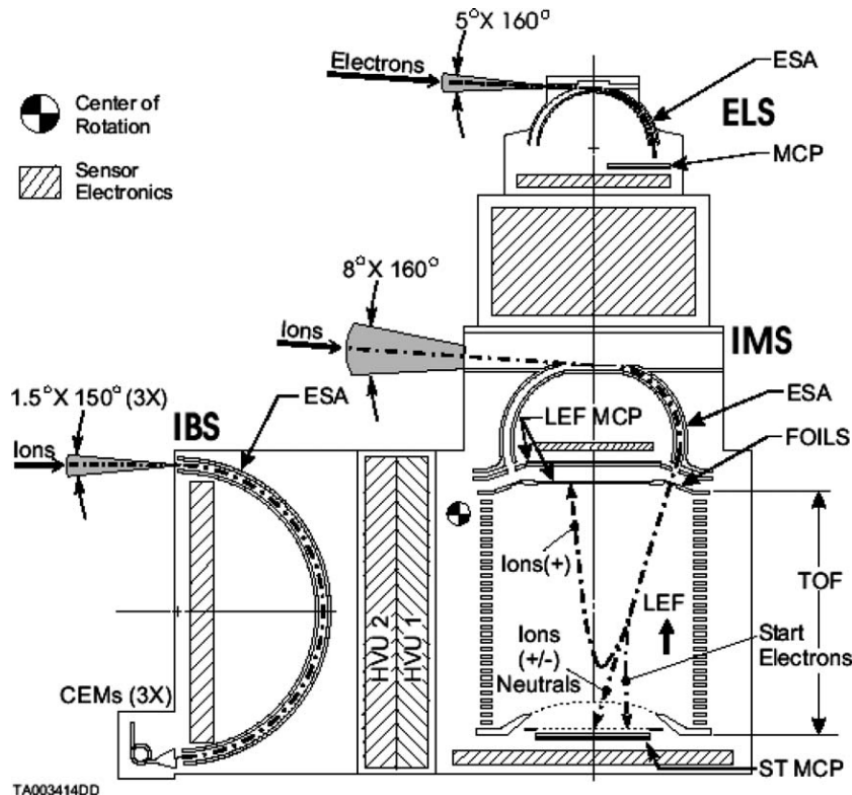


**Figure 1.8:** Diagram of the CAPS instrument, from ?. The dot-dashed lines show the general shape of particle trajectories.

curved charged plates, labelled ‘ESA’ (electrostatic analyser) in the diagram. As in the MIMI/CHEMS instrument, the voltage across the plates was stepped through a series of logarithmically spaced values over time, in order to filter only charged particles with a certain small range in  $E/Q$  at a given time.

For ELS, this corresponds to filtering for different energy electrons, as  $Q$  is fixed. The angular distribution of the incoming electrons at each energy range was then measured based on where the electrons hit the microchannel plate, labelled ‘MCP’ in Figure 1.8.

At IMS, the instrument performed time-of-flight calculations to calculate the particle energies. A linear electric field of  $-14.56\text{ kV}$  would accelerate ions that successfully exited the charged plates out into one of eight carbon foils, labelled ‘FOILS’, generating secondary electrons to be steered to a microchannel plate to measure the start time of flight, as in the MIMI/INCA and CHEMS instruments. Positive ions with energies below  $\sim 15\text{ keV}$  would

be reflected back by the linear electric field labelled ‘LEF’ into the ‘LEF MCP’, while more energetic ions would be slowed down but still eventually penetrate the ‘straight-through’ microchannel plate, labelled ‘ST MCP’. Molecular ions would break up on penetrating the carbon foils, but the resulting daughter products would still behave in this way and thus could be detected, and information used to infer the original source particle. The peaks in the observed time-of-flight spectra would correspond to given ion mass-charge ratios  $M/Q$ , such that different ion species could then be identified.

Due to a technical fault, CAPS was switched off permanently in 2012. However up until that time, observations made by the instrument were useful for investigating many magnetospheric phenomena at Saturn. Pertinent to this thesis, CAPS-ELS observations were used by ? to identify instances when *Cassini* crossed Saturn’s magnetopause boundary, from the magnetosphere into the magnetosheath, as the sheath typically contains a more dense and lower energy population of electrons than the magnetosphere. This enabled a study of how the shape and size of the magnetopause surface varied under different conditions, and is complemented by the modelling study discussed in Chapter ??.

## 1.4 Summary

The *Cassini* space mission has without a doubt revolutionised our understanding of the large-scale structure and dynamics of Saturn’s magnetosphere. Throughout this thesis, we refer to important results based on observations from these discussed *Cassini* instruments. In addition, the ? model discussed in Section ?? uses results from these instruments as equatorial boundary conditions. In the first study discussed in this thesis, we explore the influence of the variable hot plasma population detected by the MIMI instrument on the compressibility of Saturn’s dayside magnetosphere.